Acta Mech 234, 3219–3240 (2023)
https://doi.org/10.1007/s00707-023-03557-8

ORIGINAL PAPER

Yong Tao · Chu Chen · Yaser Kiani

Frequency analysis of smart sandwich cylindrical panels with nanocomposite core and piezoelectric face sheets

Received: 10 December 2022 / Revised: 6 March 2023 / Accepted: 18 March 2023 / Published online: 5 April 2023

Abstract An analysis is performed in this research to investigate the vibration response of sandwich cylindrical panels with piezoelectric layers. Core of the sandwich panel is made from a composite laminated media which is reinforced with graphene platelets. The amount of graphene in the layers may be different which results in a piecewise functionally graded media. Elasticity modulus of the core media is estimated via the Halpin–Tsai rule, while the mass density and Poisson's ratio are obtained via the simple rule of mixtures approach. By means of the first-order shear deformation panel theory and linear variation of electric field for the smart layers as the basic assumptions, the expressions of the energies of the panel are obtained. With the general idea of the Ritz method whose shape functions are constructed via the Legendre polynomials, the matrix representation of motion equations is obtained. The obtained form of equations may be used for both closed and open circuit conditions of piezoelectric layers. Results of this study are first compared with the available data in the open literature for simple cases, and after that novel numerical results are given to explore the effects of graded patterns of GPLs, weight fraction of GPLs, mechanical and electrical boundary conditions, number of layers, and also geometrical parameters. It is highlighted that frequencies may be controlled via proper graded pattern and weight fraction of GPLs. Also open circuit type of electrical boundary conditions results in higher natural frequencies in comparison to closed circuit type.

1 Introduction

Thanks to the everlasting development of nanotechnology which is led to providing super-performance composite materials, great research interest is sparked in the field of composite materials reinforced with nanoscale fillers such as nanoparticle [1], nanofiber [2, 3], CNT [4–10] and various combinations of nanofillers [11]. Revealing the remarkable superiority of graphene platelets in terms of toughness, Young's modulus, strength, etc., compared to other carbon reinforcements since its initial introduction, that is, since Novoselov et al. [12] exfoliated it from a bulk graphite in 2004, it has caused the attention of the research and industrial community. Owing to its superior mechanical properties, namely Young modulus-1TPa, ultimate strength-130 GPa and significant thermal and electrical characteristics, a very low amount of added GPLs to polymer matrix can

Y. Tao (✉) · C. Chen
Hangzhou Vocational & Technical College, Hangzhou 310018, China
e-mail: taoyong1235@163.com

C. Chen
e-mail: chenchu2025@163.com

Y. Kiani (✉)
Faculty of Engineering, Shahrekord University, Shahrekord, Iran
e-mail: y.kiani@sku.ac.ir

Y. Kiani
Nanotechnology Research Institute, Shahrekord University, Shahrekord, Iran

result in significant enhancement of properties of polymer-GPL composites, as highlighted by Rafiee et al. [13], Biswas et al. [14], Parashar and Mertiny [15]. Due to the high strength-to-weight ratio of composites reinforced with graphene platelets, it is predicted that such types of composites will be one of the most promising materials in future advent industries, especially in the aerospace industry. The mentioned items, in addition to its lower relative cost of the manufacturing process, have been the sake of the tendency of research and industrial centers to use these materials and the inspiring for conducting extensive numerical and analytical research in this realm. Due to the prevention of agglomeration and other problems in the manufacturing process, graphene platelets are generally added in a low volume percentage to polymer matrices; therefore, to increase the reinforcing efficiency, the layer-wise functionally graded distribution pattern along one or two directions may be assumed [16]. In recent years, the dynamic and static behavior of composites reinforced with functionally grade graphene platelets has been well modeled and discussed. Yang et al. assuming that the randomly oriented GPLs are used to reinforce the polymer matrix, studied bending behavior [17], buckling and post-buckling characteristics [18, 19], dynamic instability [20] and large-deflection vibrations responses [21] of functionally graded GPL-reinforced composite (FG-GPLRC) beam [20, 21], FG-GPLRC plate [18], FG-GPLRC trapezoidal plate [17] and FG-GPLRC cylindrical shell [19].

Ganapathi et al. [20] within the framework of trigonometric shear flexible model used finite element method to study the nonlinear flutter phenomenon for the functionally graded GPL-reinforced porous curved panel. Niu and his colleagues dealt with dynamic behavior of rotating pre-twisted functionally graded composite cylindrical panel. They utilized Chebyshev-Ritz method to obtain the vibration responses of the FG-GPLRC cylindrical panel. They analyzed bending response [23], thermal buckling and post-buckling [24], dynamic instability [25] and nonlinear transient response [26] of the FG-GPLRC plates [23, 25, 26], FG-GPLRC cylindrical panel and FG-GPLRC cylindrical shell [24] in thermal environments. On the basis of a variational approach, Gholami and Ansari [27] explored the primary resonant dynamics of functionally graded GPL-reinforced composites. Also, Gholami and Ansari [28] formulated the nonlinear vibrations of plates made of functionally graded graphene platelet composites using a unified higher-order shear deformable theory. Zhou et al. [29] based on a higher-order model excavated the nonlinear buckling responses of laminated composite porous cylindrical shells considering various patterns of GPLs and porosity distribution. With the aid of a Navier solution method, the effects of distribution pattern, weight fraction, geometry and size of GPLs and the effect of total number of layers on free vibration frequency of FG-GPLRC plates were analytically studied by Song et al. [30]. Baghbadorani et al. [31] exploited the first-order shear deformation theory of shells in accompany with Donnell kinematic relations to perform a free vibration frequency analysis for FG-GPLRC cylindrical shells. Esmaeili and his co-researchers through a Ritz solution method explored the free vibration characteristics of functionally graded GPLRC doubly curved panels [32]. Besides, they analyzed thermal-induced vibrations of FG-GPLRC flat plates [33] and curved panels [34].

Piezoelectric materials have played an important role in coupling the mechanical and electrical fields. To utilize in various electromechanical applications as sensors and actuators, efficient structures with superior properties can be provided by combining composite materials with piezoelectric materials. On the basis of piezoelectricity, the direct and reverse effects of piezoelectric materials is described which system controllability is oriented from. So far, to perform dynamic analysis of piezoelectric-surrounded structures, researchers have developed different mathematical approaches. To numerically predict static and dynamic behaviors of smart FG-GPLRC microplates subjected to concurrently electrical and mechanical loads, Nguyen and Lee [35] developed a numerical model on the basis of a refined plate theory, modified couple stress theory and NURBS-based isogeometric analysis. Using 3D theory of elasticity, Jalali et al. [36] investigated free vibrations of functionally graded GPL-reinforced imperfect panel surrounded with piezoelectric layers. Dong et al. [37] perused the active vibration control of sandwich thin cylindrical shells made of FG-GPLRC core and piezoelectric face sheets. They also obtained free vibration frequencies of the structure by regarding effects of the thermo-electro-elastic field. Considering a high-order shear deformation model and von Kármán terms, Lin et al. [38] obtained vibration characteristics of multilayer plates made of GPL-reinforced composite material. They also reported aeroelastic response of the plates under the action of electrical and mechanical loads. Alibeigloo and Nouri [39] obtained three-dimensional static solution of functionally graded (FG) cylindrical shell with piezoelectric layers by adopting state-space approach and implementing differential quadrature method (DQM). With the accordance of first-order shear deformation theory (FSDT), and nonlinear von Kármán assumptions, Bayat et al. [40] formulated the large-amplitude vibration control of functionally graded piezoelectric cylindrical shells subjected to concurrently axial and radial external excitations.

Jinhua et al. [41] checked bifurcation and chaos of functionally graded multilayer composite cylindrical shells with GPL reinforcements and piezoelectric layers as a result of action of a combination of electrical,

mechanical and thermal loads. Ebrahimi [42] exploited the 3D elasticity theory to present a general formula for frequency analysis of a fluid conveying composite multilayer cylindrical shell made of functionally graded material bounded with piezoelectric layers. With the accordance of a quasi-three-dimensional (3D) refined shear and normal deformation theory and through an electromechanical model, Alghanmi et al. [43] obtained bending response of functionally graded porous plates attached to a layer made of piezoelectric fiber-reinforced composite (PFRC). Such plates were under the action of sinusoidal electromechanical loads. Behavior of piezoelectric laminated composite plate exposed to various electromechanical loads was surveyed by Markad et al. [44] using the first-order shear deformation model.

The static and dynamic behaviors of panels with rectangular planform have assigned an important position in research topics in both scholar and industrial community; this importance comes from their various practical applications of these structures in various realms, including civil, mechanical, architectural, marine and aeronautical engineering. A number of theoretical analysis on such panels which performed to attain an efficient design are listed as follows:

Lore et al. [45] probed nonlinear free vibration characteristics of functionally graded plates and shell panels. Li et al. [46] investigated free vibrations of composite/sandwich shell panels. Shen and Wang [47] studied free vibrations of shear deformable FGM cylindrical panels considering the effects of thermal environment and effects of interaction between panel and elastic foundation. Viola et al. [48] used a 2D higher-order shear deformation theory to provide a general framework for dynamic investigation of doubly curved composite panels. Chen et al. [49] evaluated a novel formulation to study free vibration frequency of rotating pre-twisted laminated composite shell panels. Karimi et al. [50] in an orthogonal curvilinear coordinate system implemented higher-order model to probe forced vibration of anisotropic curved panels. Karimiasl and Alibeigloo [51] carried out free vibration analysis of composite sandwich cylindrical panels composed of double-V auxetic core and GPL-reinforced composite face sheets. In the above research, the effect of the aerohygrothermal environment was investigated. Free vibration frequencies of moderately thick cylindrical composite sandwich panels were obtained by Pourmoayed et al. [52] through an improved higher-order theory. Mohammadimehr et al. [53] discussed the parameters affecting the free vibration frequency of functionally graded CNT-reinforced magneto-electro-elastic cylindrical composite panel according to first-order shear deformation theory. Keleshteri and Jelovica [54] investigated free vibration characteristics and buckling behavior of sandwich panels made of functionally graded metal foam core surrounded with two thin face sheets.

The poor literature around free vibration analysis of FG-GPLRC cylindrical panel with piezoelectric layers is revealed with the aid of the above-presented literature review. Present study attempts to provide a numerical model with the ability of handling an arbitrary vast set of mechanical and electrical boundary conditions. Mechanical properties of the panel are approximated via Halpin–Tsai micromechanical model in accompany with the rule of mixtures. Electromechanically coupled governing equations are provided by applying Hamilton principle. Legendre-Ritz formulation is implemented to obtain discretized governing equations; accordingly, natural frequencies are calculated. The rest of article deals with validating present model and subsequently performing parametric studies. As shown for different combinations of edge supports, various GPL weight fractions and patterns, open circuit type of edge support results in higher frequencies.

2 Problem description

The functionally graded GPL-reinforced cylindrical panel surrounded with two identical piezoelectric layers is under free vibration analysis with details as follows. Its geometrical properties are symbolized as follows: length of straight edge: a, length of curved edge: b, radius of curvature: R and total thickness of panel: $h+2h^p$ where h^p is the thickness of piezoelectric layer and h is the thickness of the core. Figure 1 also provides a schematic of the structure.

It is assumed that an even number of GPL-reinforced layers (N_L) of the same size, arranged according to a mathematical function are composed the panel. Besides, uniform dispersion and random orientation for GPLs in each layer is considered. To describe deformations and displacements, a curvilinear coordinate system mounted on mid-plane of the panel in such a way that it describes the panel domain as: $-0.5a \leq x_1 \leq 0.5a$, $-0.5b \leq x_2 \leq 0.5b$ and $-0.5h - h^p \leq x_3 \leq 0.5h + h^p$ is considered.

Several types of GPL distribution profiles through the thickness may be assumed. Herein, the following distribution patterns with linear variations of GPL weight fraction from layer to layer are taken to account. Such patterns are demonstrated in Fig. 2 and are listed as:

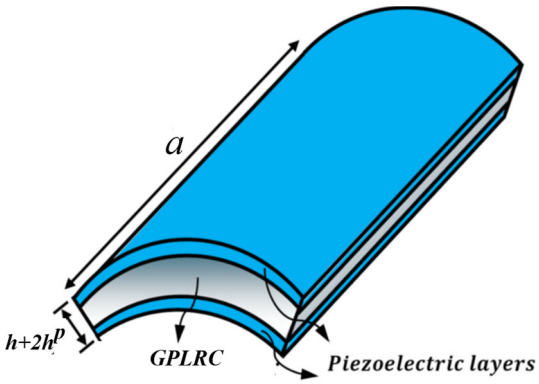

Fig. 1 Schematic of the structure composed of GPLRC core and piezoelectric faces

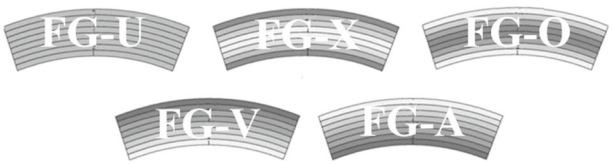

Fig. 2 Layer-wise functionally graded GPL distribution patterns

(a) FG-U
Here, monotonic dispersion of GPLs through the panel thickness is assumed. Accordingly, we will deal with an isotropic and homogeneous cylindrical panel, i.e.,

$$V_{GPL}^{(k)} = V_{GPL}^{*} \quad (k = 1, 2, \ldots, N_L) \tag{1}$$

(b) FG-X
Based on this pattern, the layers with the highest GPL volume fraction are located in the top and bottom surfaces, while GPL-poor layers can be found in mid-surfaces. This pattern is symmetrical with respect to the mid-plane, i.e.,

$$V_{GPL}^{(k)} = 2V_{GPL}^{*}\frac{|2k - N_L - 1|}{N_L} \quad (k = 1, 2, \ldots, N_L) \tag{2}$$

(c) FG-O
In this pattern, the positions of the GPL-rich and GPL-poor layers are completely in contrary to what was outlined about the FG-X pattern. For instance, GPL volume fraction is the lowest at top and bottom, i.e.,

$$V_{GPL}^{(k)} = 2V_{GPL}^{*}\left(1 - \frac{|2k - N_L - 1|}{N_L}\right) \quad (k = 1, 2, \ldots, N_L) \tag{3}$$

(d) FG-V
Next pattern which is an asymmetric pattern with respect to the middle plane provides the maximum amount of GPLs at top and its minimum at bottom, i.e.,

$$V_{GPL}^{(k)} = V_{GPL}^{*}\frac{2k - 1}{N_L} \quad (k = 1, 2, \ldots, N_L) \tag{4}$$

(e) FG-A
The last pattern, which is again an asymmetric pattern, is defined as linearly increasing variation of GPL volume fraction from top to bottom surface, i.e.,

$$V_{GPL}^{(k)} = V_{GPL}^{*}\frac{-2k + 1 + 2N_L}{N_L} \quad (k = 1, 2, \ldots, N_L) \tag{5}$$

The above relationships provide the GPL volume fraction of the k-th layer ($V_{GPL}^{(k)}$) in terms of the total GPL volume fraction of the FG-GPLRC panel (V_{GPL}^{*}).

The relationship between the GPL volume fraction (V_{GPL}^{*}) and the GPL weight fraction (W_{GPL}^{*}) having the density ratio (ρ_{GPL}/ρ_m) is expressed as follows [31]

$$V_{GPL}^{*} = \frac{W_{GPL}}{W_{GPL} + \frac{\rho_{GPL}}{\rho_m}(1 - W_{GPL})} \tag{6}$$

By having the GPL volume fraction in each layer, the mechanical properties can be calculated.

First, Young's modulus is estimated exploiting the Voigt–Reuss model as:

$$E^{(k)} = \frac{3}{8}E_1^{(k)} + \frac{5}{8}E_2^{(k)} \tag{7}$$

Longitudinal modulus $E_1^{(k)}$ and transverse modulus $E_2^{(k)}$ are approximated via the Halpin–Tsai micromechanical model which is modified to include the effects of size and geometry of nanoscale fillers [31].

$$\begin{aligned} E_1^{(k)} &= \frac{1 + \xi_L \eta_L V_{GPL}^{(k)}}{1 - \eta_L V_{GPL}^{(k)}} E_m \\ E_2^{(k)} &= \frac{1 + \xi_T \eta_T V_{GPL}^{(k)}}{1 - \eta_T V_{GPL}^{(k)}} E_m \end{aligned} \tag{8}$$

where

$$\eta_L = \frac{E_{GPL} - E_m}{E_{GPL} + \xi_L E_m} \eta_T = \frac{E_{GPL} - E_m}{E_{GPL} + \xi_T E_m} \tag{9}$$

Here, the elastic moduli are represented by E_m and E_{GPL}, corresponding to the matrix and GPL, respectively. Also, ξ_L and ξ_T are two parameters that include both GPL size and geometry effects [31].

$$\xi_L = 2\frac{l_{GPL}}{h_{GPL}} \xi_T = 2\frac{w_{GPL}}{h_{GPL}} \tag{10}$$

w_{GPL}, l_{GPL} and h_{GPL} in above are used for average width, length, and thickness of GPLs, respectively.

Next, the law of mixtures is utilized to calculate density and Poisson's ratio of the composite media as [31]

$$\begin{aligned} \nu^{(k)} &= \nu_m\left(1 - V_{GPL}^{(k)}\right) + \nu_{GPL} V_{GPL}^{(k)} \\ \rho^{(k)} &= \rho_m\left(1 - V_{GPL}^{(k)}\right) + \rho_{GPL} V_{GPL}^{(k)} \end{aligned} \tag{11}$$

3 Mathematic model derivation

Different theories may be used to estimate and model the displacement in beams, plates and shell, see, e.g., [55–63]. Considering the piezoelectric layers leads to dealing with a moderately thick panel, hence, the first-order shear deformation model (FSDT) is the most optimal choice to describe the displacement field, accordingly [32–34],

$$\mathbf{U} = \begin{Bmatrix} U_1(x_1, x_2, x_3, t) \\ U_2(x_1, x_2, x_3, t) \\ U_3(x_1, x_2, x_3, t) \end{Bmatrix} = \begin{Bmatrix} u(x_1, x_2, t) + x_3\theta_1(x_1, x_2, t) \\ v(x_1, x_2, t) + x_3\theta_2(x_1, x_2, t) \\ w(x_1, x_2, t) \end{Bmatrix} \tag{12}$$

The projections of displacement on the mid-plane along with x_1-, x_1- and x_3-axes are represented by u, v and w, respectively. Besides, θ_1 and θ_2 signify to rotations of transverse normal about x_2- and x_1-axes, respectively.

On the basis of given displacement field, one can present linear strain–displacement relations as follows for the in-plane strains

$$\begin{aligned}
\varepsilon_{11} &= U_{1,x_1} = \varepsilon_{11}^0 + x_3\kappa_1 = u_{,x_1} + x_3\theta_{1,x_1} \\
\varepsilon_{22} &= U_{2,x_2} = \varepsilon_{22}^0 + x_3\kappa_1 = v_{,x_1} + \frac{w}{R} + x_3\theta_{2,x_2} \\
\varepsilon_{12} &= U_{1,x_2} + U_{2,x_1} = \varepsilon_{12}^0 + x_3\kappa_{12} = u_{,x_2} + v_{,x_1} + x_3\left(\theta_{1,x_2} + \theta_{2,x_1}\right) \\
\varepsilon_{23} &= \varepsilon_{23}^0 = \theta_2 + w_{,x_2} \\
\varepsilon_{13} &= \varepsilon_{13}^0 = \theta_1 + w_{,x_1}
\end{aligned} \tag{13}$$

In above relations and hereafter, (,) stands for differential operator.

4 Constitutive relations

4.1 Constitutive relations of GPLRC layers

For GPLRC layers, Hooke law compatible with the conditions of zero value for $\sigma_{33}^{(k)}$ states that stress vector, $\boldsymbol{\sigma}^{(k)} = [\sigma_{11}^{(k)}, \sigma_{22}^{(k)}, \sigma_{12}^{(k)}, \sigma_{13}^{(k)}, \sigma_{23}^{(k)}]^{\boldsymbol{T}}$ and strain vector, $\boldsymbol{\varepsilon} = [\varepsilon_{11}.\varepsilon_{22}, 2\varepsilon_{12}, 2\varepsilon_{13}, 2\varepsilon_{23}]^T$ are related by the following relation:

$$\boldsymbol{\sigma}^{(k)} = \mathbf{C}^{(k)}\boldsymbol{\varepsilon} \tag{14}$$

$\mathbf{C}^{(k)}$ is the elastic constant matrix for the k-th GPLRC layer.

$$\begin{aligned}
\mathbf{C}^{(k)} &= \begin{bmatrix} \mathbf{C}_1^{(\mathrm{k})} & 0 \\ 0 & \mathbf{C}_2^{(\mathrm{k})} \end{bmatrix} \\
\mathbf{C}_1^{(\mathrm{k})} &= \frac{E^{(k)}}{1-\upsilon^{(k)2}} \begin{bmatrix} 1 & \upsilon^{(k)} & 0 \\ \upsilon^{(k)} & 1 & 0 \\ 0 & 0 & \frac{1-\upsilon^{(k)}}{2} \end{bmatrix}, \\
\mathbf{C}_2^{(\mathrm{k})} &= \frac{E^{(k)}}{2\left(1+\upsilon^{(k)}\right)} \begin{bmatrix} 1 & 0 \\ 0 & 1 \end{bmatrix}
\end{aligned} \tag{15}$$

4.2 Constitutive relations of top and bottom piezoelectric layers

In view of the piezoelasticity theory, the constitutive relation of piezoelectric layers may be written as:

$$\begin{Bmatrix} \boldsymbol{\sigma}^{\mathbf{p}} \\ \mathbf{D} \end{Bmatrix} = \begin{bmatrix} \mathbf{C}^{\mathbf{p}} & -\mathbf{e}^T \\ \mathbf{e} & \boldsymbol{\Xi} \end{bmatrix} \begin{Bmatrix} \boldsymbol{\varepsilon} \\ \mathbf{E} \end{Bmatrix} \tag{16}$$

In Eq. (16), $\mathbf{C}^{\mathbf{p}}$ signifies the elastic constant matrix for the piezoelectric layers, $\boldsymbol{\Xi}$ is the dielectric permittivity constant matrix and $\mathbf{e}$ represents the electromechanical coupling matrix; accordingly, they have following definition:

$$\mathbf{C}^{\mathbf{p}} = \begin{pmatrix} \overline{Q}_{11}^p & \overline{Q}_{12}^p & 0 & 0 & 0 \\ \overline{Q}_{12}^p & \overline{Q}_{22}^p & 0 & 0 & 0 \\ 0 & 0 & \overline{Q}_{66}^p & 0 & 0 \\ 0 & 0 & 0 & Q_{44}^p & 0 \\ 0 & 0 & 0 & 0 & Q_{55}^p \end{pmatrix}$$

$$\mathbf{e}=\begin{bmatrix} 0 & 0 & 0 & e_{15} & 0 \\ 0 & 0 & e_{15} & 0 & 0 \\ \overline{e}_{31} & \overline{e}_{31} & 0 & 0 & 0 \end{bmatrix}$$
$$\mathbf{\Xi}=\begin{bmatrix} \Xi_{11} & 0 & 0 \\ 0 & \Xi_{22} & 0 \\ 0 & 0 & \overline{\Xi}_{33} \end{bmatrix} \tag{17}$$

Elastic matrix components related to piezoelectric material are presented as

$$\overline{Q}^p_{11}=\overline{Q}^p_{22}=Q^p_{11}-\frac{Q^p_{13}Q^p_{13}}{Q^p_{33}},\quad \overline{Q}^p_{12}=Q^p_{12}-\frac{Q^p_{13}Q^p_{13}}{Q^p_{33}},\quad \overline{Q}^p_{66}=\frac{1}{2}\left(\overline{Q}^p_{11}-\overline{Q}^p_{12}\right)$$
$$\overline{e}_{31}=e_{31}-\frac{Q^p_{13}}{Q^p_{33}}e_{33},\quad \overline{\Xi}_{33}=\Xi_{33}+\frac{e^2_{33}}{Q^p_{33}} \tag{18}$$

Also, $\boldsymbol{\sigma^p}$, **E** and **D** represent the stress field in piezoelectric layers compatible with the condition of absence of σ^p_{33}, the electrical field and the electrical displacement field, respectively, and may be written as:

$$\boldsymbol{\sigma}^{\mathrm{p}}=\left[\sigma^p_{11},\sigma^p_{22},\sigma^p_{12},\sigma^p_{23},\sigma^p_{13}\right]^{\boldsymbol{T}}$$
$$\mathbf{D}=[D_1,D_2,D_3]^{\boldsymbol{T}}$$
$$\mathbf{E}=[E_1,E_2,E_3]^{\boldsymbol{T}}=-\left[\Phi_{,x_1},\Phi_{,x_2},\Phi_{,x_3}\right]^{\boldsymbol{T}} \tag{19}$$

where Φ is electrical potential function which in accordance with the electrical boundary conditions will be specified in follow.

The relatively thin piezoelectric layers make it reasonable to assume the linearity of the electric potential changes along the thickness of the piezoelectric layers. Hereupon, the electrical potential function in top and bottom piezoelectric layers can be read as:

$$\Phi(x_1,x_2,x_3)=\begin{cases} \frac{x_3-0.5h}{h^p}\varphi^t(x_1,x_2) 0.5h<z<0.5h+h^p \\ -\frac{x_3+0.5h}{h^p}\varphi^b(x_1,x_2)-0.5h-h^p<z<-0.5h \end{cases} \tag{20}$$

As applied in the above relation, it is assumed that the surface of piezoelectric layers bordering GPLRC layers is grounded; accordingly, the electrical potential at this surface is equal to zero.

The governing equations are obtained by exploiting the Hamilton's principle that for the under consideration problem is extended in the following form [41]:

$$\int_0^t(\delta U-\delta T)\mathrm{d}t=0 \tag{21}$$

where t is an arbitrary time. Also the variations of strain energy, δU and kinetic energy, δT for the cylindrical shell panel are calculated as:

$$\delta U=\int_{-0.5b}^{0.5b}\int_{-0.5a}^{0.5a}\sum_{k=1}^{N_L}\int_{h_{k-1}}^{h_k}\left(\sigma^{(k)}_{11}\delta\varepsilon_{11}+\sigma^{(k)}_{22}\delta\varepsilon_{22}+2\sigma^{(k)}_{12}\delta\varepsilon_{12}+2\kappa^{(k)}_s\sigma^{(k)}_{23}\delta\varepsilon_{23}+2\kappa^{(k)}_s\sigma^{(k)}_{13}\delta\varepsilon_{13}\right)\mathrm{d}x_3\mathrm{d}x_1\mathrm{d}x_2$$
$$+\int_{-0.5b}^{0.5b}\int_{-0.5a}^{0.5a}\int_{0.5h}^{0.5h+0.5h^p}(\sigma^p_{11}\delta\varepsilon_{11}+\sigma^p_{22}\delta\varepsilon_{22}+2\sigma^p_{12}\delta\varepsilon_{12}+2\kappa^p_s\sigma^p_{23}\delta\varepsilon_{23}+2\kappa^p_s\sigma^p_{13}\delta\varepsilon_{13}-D_1\delta E_1-D_2\delta E_2$$

$$
\begin{aligned}
&- D_3\delta E_3)\mathrm{d}x_3\mathrm{d}x_1\mathrm{d}x_2 \\
&+ \int_{-0.5b}^{0.5b}\int_{-0.5a}^{0.5a}\int_{-0.5h-0.5h^p}^{-0.5h} (\sigma_{11}^p\delta\varepsilon_{11} + \sigma_{22}^p\delta\varepsilon_{22} + 2\sigma_{12}^p\delta\varepsilon_{12} + 2\kappa_s^p\sigma_{23}^p\delta\varepsilon_{23} + 2\kappa_s^p\sigma_{13}^p\delta\varepsilon_{13} \\
&- D_1\delta E_1 - D_2\delta E_2 - D_3\delta E_3)\mathrm{d}x_3\mathrm{d}x_1\mathrm{d}x_2 \\
\delta T = &\int_{-0.5b}^{0.5b}\int_{-0.5a}^{0.5a}\sum_{k=1}^{N_L}\int_{h_{k-1}}^{h_k}\left(\rho^{(k)}\left\{\dot{U}_1[\delta\dot{u} + x_3\delta\theta_1] + \dot{U}_2[\delta\dot{v} + x_3\delta\theta_2] + \dot{U}_3\delta\dot{w}\right\}\right)\mathrm{d}x_3\mathrm{d}x_1\mathrm{d}x_2 \\
&+ \int_{-0.5b}^{0.5b}\int_{-0.5a}^{0.5a}\int_{0.5h}^{0.5h+0.5h^p}\left(\rho^p\left\{\dot{U}_1[\delta\dot{u} + x_3\delta\theta_1] + \dot{U}_2[\delta\dot{v} + x_3\delta\theta_2] + \dot{U}_3\delta\dot{w}\right\}\right)\mathrm{d}x_3\mathrm{d}x_1\mathrm{d}x_2 \\
&+ \int_{-0.5b}^{0.5b}\int_{-0.5a}^{0.5a}\int_{-0.5h-0.5h^p}^{-0.5h}\left(\rho^p\left\{\dot{U}_1[\delta\dot{u} + x_3\delta\theta_1] + \dot{U}_2[\delta\dot{v} + x_3\delta\theta_2] + \dot{U}_3\delta\dot{w}\right\}\right)\mathrm{d}x_3\mathrm{d}x_1\mathrm{d}x_2
\end{aligned}
\tag{22}
$$

In above, $\kappa_s^{(k)}$ and κ_s^p are the shear correction factor of k-th GPLRC layer and piezoelectric layers, respectively. They are considered as:

$$
\begin{aligned}
\kappa_s^p &= \frac{5}{6} \\
\kappa_s^{(k)} &= \frac{5}{\left(6 - \upsilon_m^{(k)}V_m^{(k)} - \upsilon_{GPL}^{(k)}V_{GPL}^{(k)}\right)}
\end{aligned}
\tag{23}
$$

5 Solution method

The strong form of the equations of motion along with Maxwell's equations can be derived by applying the Green theorem to Eq. (21). But in current work, energy-based methods are employed to present a comprehensive formulation for a wide set of boundary conditions. The Ritz method, as one of the energy-based methods, has demonstrated its competence in solving solid mechanics problems due to its high accuracy, fast convergence, and uncomplicated formulation that can be easily implemented. Hence, Ritz method on the basis of Legendre-type polynomials is implemented to attain the matrix representation of governing motion equations and Maxwell equations. Accordingly, each of the independent variables is expanded by means of a double series of a combination of two one-dimensional admissible functions [32–34]

$$
\begin{Bmatrix}
u(x_1x_2,t) \\ v(x_1x_2,t) \\ w(x_1x_2,t) \\ \theta_1(x_1x_2,t) \\ \theta_2(x_1x_2,t) \\ \varphi^t(x_1x_2,t) \\ \varphi^b(x_1x_2,t)
\end{Bmatrix}
= \sum_{n=0}^{N_{x_1}}\sum_{m=0}^{N_{x_2}}
\begin{Bmatrix}
U_{nm}(t) \\ V_{nm}(t) \\ W_{nm}(t) \\ X_{nm}(t) \\ Y_{nm}(t) \\ T_{nm}(t) \\ B_{nm}(t)
\end{Bmatrix}
\Gamma_n(x_1)\Gamma_m(x_2)
\tag{24}
$$

N_{x_1} and N_{x_2} specify the number of trial terms; besides, the one-dimensional admissible functions $\Gamma_n(x_1)$ and $\Gamma_m(x_2)$ are defined as the product of the n-th and m-th-order Legendre polynomials ($L_n(x_1)$, $L_m(x_2)$) to boundary functions ($\xi^\alpha(x_1)$, $\varsigma^\alpha(x_2)$) which are made in compatible with the essential boundary conditions

Table 1 Value of $\chi_s^{\alpha}(\alpha = \text{u, v, w, } \theta_1, \theta_2 \text{ and s} = 1, 2, 3, 4)$ for SCSF panel

χ_s^u	χ_s^v	χ_s^w	$\chi_s^{\theta_1}$	$\chi_s^{\theta_2}$
(0, 1, 0,0)	(1, 1, 1, 0)	(1, 1, 1, 0)	(0, 1, 0, 0)	(1, 1, 1, 0)

$$\begin{aligned}\Gamma_n(x_1) &= L_n(x_1)\xi^{\alpha}(x_1)\\ \Gamma_m(x_2) &= L_m(x_2)\varsigma^{\alpha}(x_1)\\ &\left(\alpha = u, v, w, \theta_1, \theta_2, \varphi^t, \varphi^b\right)\end{aligned} \tag{25}$$

where Legendre polynomials read as:

$$\begin{aligned}L_0(x_1) &= L_0(x_2) = 1\\ L_1(x_1) &= \frac{2x_1}{a},\ L_1(x_2) = \frac{2x_2}{b}\\ L_{n+1}(x_1) &= \frac{(2n+1)\frac{2x_1}{a}L_n(x_1) - nL_{n-1}(x_1)}{n+1}\\ L_{m+1}(x_2) &= \frac{(2m+1)\frac{2x_2}{b}L_m(x_2) - mL_{m-1}(x_2)}{m+1}\end{aligned} \tag{26}$$

Boundary functions are proposed as the following general form to have the ability to easily update for the desired combination of boundary conditions:

$$\begin{aligned}\xi^{\alpha}(x_1) &= \left(1 + \frac{2x_1}{a}\right)^{\chi_1^{\alpha}}\left(1 - \frac{2x_1}{a}\right)^{\chi_2^{\alpha}}\\ \varsigma^{\alpha}(x_2) &= \left(1 + \frac{2x_2}{b}\right)^{\chi_3^{\alpha}}\left(1 - \frac{2x_2}{b}\right)^{\chi_4^{\alpha}}\end{aligned} \tag{27}$$

χ_i^{α} are the auxiliary parameters that must be assigned a value of zero or one in such a way as to enable the boundary function to satisfy the essential boundary conditions. In present work, sets of clamped (C), simply supported (S) and free (F) edges are considered. It should to be noted a conventional notation convention for citing boundary conditions is established upon which for an instance, a panel with simply supported edge at $x = -a/2$, clamped edge at $y = -b/2$, simply supported edge at $x = a/2$ and free edge at $y = b/2$ is cited as "SCSF panel". The cells of Table 1 are filled with values of χ_s^{α} $(\alpha = u,\ v,\ w,\ \theta_1,\ \theta_2 \text{ and } s = 1, 2, 3, 4)$ as an example for SCSF panel.

The electrical displacement and the electrical field in all four edges of each of the two piezoelectric layers are considered equal to zero. (It is assumed that piezoelectric layers are grounded on all four edges.) Therefore, the electrical boundary conditions for the piezoelectric layers may be expressed as:

$$\begin{aligned}&\varphi^t(x_1, x_2) = 0 \text{ at } (0.5a, x_2), (-0.5a, x_2), (x_1, 0.5b) \text{ and } (x_1, -0.5b)\\ &\varphi^b(x_1, x_2) = 0 \text{ at } (0.5a, x_2), (-0.5a, x_2), (x_1, 0.5b) \text{ and } (x_1, -0.5b)\end{aligned} \tag{28}$$

In view of the electrical boundary conditions and considering that the Legendre polynomials are not zero at the boundaries, the boundary functions should be selected in such a way that they satisfy the electrical boundary conditions, accordingly:

$$\begin{aligned}\xi^{\alpha}(x_1) &= \left(1 + \frac{2x_1}{a}\right)\left(1 - \frac{2x_1}{a}\right)\\ \varsigma^{\alpha}(x_2) &= \left(1 + \frac{2x_2}{b}\right)\left(1 - \frac{2x_2}{b}\right)\quad \alpha = \varphi^t, \varphi^b\end{aligned} \tag{29}$$

By introducing the series expansion (24) into Eq. (21) and performing integration over the domain, the variations of essential variables are relived. Subsequently, a total of 7 $N_{x_1}N_{x_2}$ equations which contain unknown time-dependent functions are attained which can be recast in matrix form as:

$$\mathbf{M}\ddot{\mathbf{\Delta}} + \mathbf{K}\mathbf{\Delta} = 0 \tag{30}$$

where $\mathbf{M}$ and $\mathbf{K}$ are inertia and stiffness matrices, respectively. Besides, $\boldsymbol{\Delta}$ represents unknown vector which contains $U_{nm}(t)$, $V_{nm}(t)$, $W_{nm}(t)$, $X_{nm}(t)$, $Y_{nm}(t)$, $T_{nm}(t)$ and $B_{nm}(t)$. These set also may be presented as:

$$\mathbf{M} = \begin{bmatrix} \mathbf{M^{XX}} & \mathbf{M^{XE}} \\ \mathbf{M^{EX}} & \mathbf{M^{EE}} \end{bmatrix}, \mathbf{K} = \begin{bmatrix} \mathbf{K^{XX}} & \mathbf{K^{XE}} \\ \mathbf{K^{EX}} & \mathbf{K^{EE}} \end{bmatrix}, \boldsymbol{\Delta} = \begin{Bmatrix} \boldsymbol{\Delta}^{\mathbf{X}} \\ \boldsymbol{\Delta}^{\mathbf{E}} \end{Bmatrix} \tag{31}$$

The other above-mentioned matrices read as:

$$\begin{aligned}
\mathbf{M^{EX}} &= \mathbf{M^{XE}} = \mathbf{M^{EE}} = 0 \\
\mathbf{M}^{XX} &= \begin{bmatrix} \mathbf{M}^{uu} & \mathbf{M}^{uv} & \mathbf{M}^{u\theta_1} & \mathbf{M}^{u\theta_2} & \mathbf{M}^{uw} \\ \mathbf{M}^{vu} & \mathbf{M}^{vv} & \mathbf{M}^{v\theta_1} & \mathbf{M}^{v\theta_2} & \mathbf{M}^{vw} \\ \mathbf{M}^{\theta_1 u} & \mathbf{M}^{\theta_1 v} & \mathbf{M}^{\theta_2\theta_1} & \mathbf{M}^{\theta_1\theta_2} & \mathbf{M}^{\theta_2 w} \\ \mathbf{M}^{\theta_2 u} & \mathbf{M}^{\theta_2 v} & \mathbf{M}^{\theta_2\theta_1} & \mathbf{M}^{\theta_2\theta_2} & \mathbf{M}^{\theta_2 w} \\ \mathbf{M}^{wu} & \mathbf{M}^{wv} & \mathbf{M}^{w\theta_1} & \mathbf{M}^{w\theta_2} & \mathbf{M}^{ww} \end{bmatrix} \\
\mathbf{K}^{XX} &= \begin{bmatrix} \mathbf{K}^{uu} & \mathbf{K}^{uv} & \mathbf{K}^{u\theta_1} & \mathbf{K}^{u\theta_2} & \mathbf{K}^{uw} \\ \mathbf{K}^{vu} & \mathbf{K}^{vv} & \mathbf{K}^{v\theta_1} & \mathbf{K}^{v\theta_2} & \mathbf{K}^{vw} \\ \mathbf{K}^{\theta_1 u} & \mathbf{K}^{\theta_1 v} & \mathbf{K}^{\theta_2\theta_1} & \mathbf{K}^{\theta_1\theta_2} & \mathbf{K}^{\theta_2 w} \\ \mathbf{K}^{\theta_2 u} & \mathbf{K}^{\theta_2 v} & \mathbf{K}^{\theta_2\theta_1} & \mathbf{K}^{\theta_2\theta_2} & \mathbf{K}^{\theta_2 w} \\ \mathbf{K}^{wu} & \mathbf{K}^{wv} & \mathbf{K}^{w\theta_1} & \mathbf{K}^{w\theta_2} & \mathbf{K}^{ww} \end{bmatrix} \\
\mathbf{K}^{XE} &= \begin{bmatrix} \mathbf{K}^{\mathbf{u}\boldsymbol{\varphi}^t} & \mathbf{K}^{\mathbf{v}\boldsymbol{\varphi}^t} & \mathbf{K}^{\mathbf{w}\boldsymbol{\varphi}^t} & \mathbf{K}^{\boldsymbol{\theta}_1\boldsymbol{\varphi}^t} & \mathbf{K}^{\boldsymbol{\theta}_2\boldsymbol{\varphi}^t} \\ \mathbf{K}^{\mathbf{u}\boldsymbol{\varphi}^b} & \mathbf{K}^{\mathbf{v}\boldsymbol{\varphi}^b} & \mathbf{K}^{\mathbf{w}\boldsymbol{\varphi}^b} & \mathbf{K}^{\boldsymbol{\theta}_1\boldsymbol{\varphi}^b} & \mathbf{K}^{\boldsymbol{\theta}_2\boldsymbol{\varphi}^b} \end{bmatrix}^{\mathrm{T}} \\
\mathbf{K}^{\mathrm{EX}} &= \begin{bmatrix} \mathbf{K}^{\boldsymbol{\varphi}^t u} & \mathbf{K}^{\boldsymbol{\varphi}^t v} & \mathbf{K}^{\boldsymbol{\varphi}^t w} & \mathbf{K}^{\boldsymbol{\varphi}^t\boldsymbol{\theta}_1} & \mathbf{K}^{\boldsymbol{\varphi}^t\boldsymbol{\theta}_2} \\ \mathbf{K}^{\boldsymbol{\varphi}^b u} & \mathbf{K}^{\boldsymbol{\varphi}^b v} & \mathbf{K}^{\boldsymbol{\varphi}^b w} & \mathbf{K}^{\boldsymbol{\varphi}^b\boldsymbol{\theta}_1} & \mathbf{K}^{\boldsymbol{\varphi}^b\boldsymbol{\theta}_2} \end{bmatrix} \\
\mathbf{K}^{\mathrm{EE}} &= \begin{bmatrix} \mathbf{K}^{\boldsymbol{\varphi}^t\boldsymbol{\varphi}^t} & \mathbf{K}^{\boldsymbol{\varphi}^b\boldsymbol{\varphi}^t} \\ \mathbf{K}^{\boldsymbol{\varphi}^t\boldsymbol{\varphi}^b} & \mathbf{K}^{\boldsymbol{\varphi}^b\boldsymbol{\varphi}^b} \end{bmatrix}
\end{aligned} \tag{32}$$

By merging two above matrix equations, one can obtain a single equation to predict vibration behavior of FG-GPLRC panel surrounded with piezoelectric layers

$$\mathbf{M}^{XX}\ddot{\boldsymbol{\Delta}}^{X} + \mathbf{K^{e}}\boldsymbol{\Delta}^{X} = 0 \tag{33}$$

Here, recast stiffness matrix has the following definition:

$$\mathbf{K^{e}} = \mathbf{K^{XX}} - \mathbf{K^{XE}}\mathbf{K^{EE}}^{-1}\mathbf{K^{EX}} \tag{34}$$

Since we are dealing with a free vibration problem, the solution to the problem will be in the form of $\boldsymbol{\Delta}^{X} = \boldsymbol{\delta}\cos(\omega t + \beta)$, where ω is the natural frequency. By substituting the solution in Eq. (33), we attain an eigenvalue problem as:

$$(\mathbf{K^{e}} - \omega^2\mathbf{M}^{XX})\boldsymbol{\delta} = 0 \tag{35}$$

It is worth noting, in current research, two types of electrical boundary conditions, namely closed circuit and open circuit, are taken into account. Based upon the open circuit electrical boundary conditions, electrical potentials at free surface of piezoelectric layers are non-zero unknowns. In closed circuit case, it's assumed that top and bottom surfaces of the both piezoelectric layers are grounded so $\mathbf{K^{e}} = \mathbf{K^{EE}}$.

Non-trivial solutions of Eq. (35) are the natural frequencies of FG-GPLRC panel bounded with piezoelectric layers.

Table 2 Comparison of frequencies in Hertz ($\omega^* = \omega/2\pi$) between our results and those of Olson and Lindberg [64] for the case of fully clamped isotropic homogeneous panel

	Present	Olson and Lindberg [64]
ω_1^*	869	814
ω_2^*	958	940
ω_3^*	1287	1260
ω_4^*	1363	1306
ω_5^*	1439	1452
ω_6^*	1752	1770
ω_7^*	1777	1802
ω_8^*	2056	2100
ω_9^*	2218	2225
ω_{10}^*	2286	2280

6 Results and discussion

To perform numerical studies on free vibration of functionally graded GPL-reinforced cylindrical panel integrated with piezoelectric layers, the following mechanical properties for Epoxy matrix and GPL reinforcement (with $l_{GPL} = 2.5\mu m$, $w_{GPL} = 1.5\mu m$ and $h_{GPL} = 1.5\mu m)\mu m$ are considered

$$E_{GPL} = 1010\,\text{GPa}, \quad \rho_{GPL} = 1062.5\frac{\text{kg}}{\text{m}^3}, \quad \nu_{GPL} = 0.186$$
$$E_m = 3\,\text{GPa}, \quad \rho_m = 1200\frac{\text{kg}}{\text{m}^3}, \quad \nu_m = 0.34 \tag{36}$$

It is assumed that PZT-4 is used as top and bottom piezoelectric layers; accordingly, the following electromechanical properties for piezoelectric layers are taken into account:

$$Q_{11}^p = 132\,\text{GPa},\ Q_{12}^p = 71\,\text{GPa},\ Q_{33}^p = 115\,\text{GPa},\ Q_{13}^p = 73\,\text{GPa},\ Q_{55}^p = 26\,\text{GPa}\,\rho^p = 7500\frac{\text{kg}}{\text{m}^3},$$
$$e_{31} = e_{32} = -4.1\frac{C}{m^2}, e_{15} = e_{24} = 10.5\frac{C}{m^2}, e_{33} = 14.1\frac{C}{m^2}, \Xi_{11} = \Xi_{22} = 7.124\frac{nF}{m} \text{ and}$$
$$\Xi_{33} = 5.841\,nF/m \tag{37}$$

Besides, if no other value is mentioned, the following geometrical specifications are used:

$$\frac{a}{b} = 1, \frac{a}{h} = 20, \frac{R}{a} = 5, \frac{h^p}{h} = 0.05 \tag{38}$$

One of the main factors which affects the numerical results in Ritz method is the number of shape functions. In the open literature this factor is analyzed as a convergence study. Previous research from the third author of this study [5] reveals that when the number of shape functions is set equal to 14 in each direction, accurate results are achieved for free vibrations of cylindrical panels. As a result, the number of shape functions is set equal to 14 in each direction of the panel for all of the results.

Herein, the first subsection aims to show the validity and accuracy of the present formulation and the numerical results subsequently.

First comparison of this study is devoted to experimental results. The case of an isotropic homogeneous cylindrical panel is considered with all edges clamped where the geometrical characteristics are $b = 0.0762\,\text{m}$, $a = 0.1016\,\text{m}$, $h = 0.03302\,\text{cm}$, $R = 0.762\,\text{m}$, $E = 68.947\,\text{GPa}$, $\rho = 2657.27\,\text{kg}/m^3$, $\nu = 0.33$. Comparison is performed in Table 2. First ten frequencies in Hertz are obtained and compared with those of Olson and Lindberg [64]. It is seen that results are in close agreement.

The second comparison case is established in such a way that fundamental frequency parameters ($\Omega = \omega a^2/h\sqrt{\rho_m/E_m}$) of completely clamped (CCCC) FG-GPLRC cylindrical shell panel for various values of

Table 3 Validation of the first frequency parameter Ω of CCCC FG-GPLRC cylindrical panel

a/h	R/a	Epoxy		UD		FG-X		FG-O		FG-A	
		Present	Ref. [65]	Present	Ref. [65]	Present	Ref. [65]	Present	Ref. [65]	Present	Ref. [65]
20	5	11.2991	11.3115	23.4889	23.5359	26.8745	26.6760	19.3561	19.4226	21.4160	21.4637
	10	10.8712	10.8810	22.5992	22.6400	26.1007	25.8854	18.2662	18.3299	20.4491	20.4855
	20	10.7614	10.7705	22.3708	22.4100	25.9034	25.6836	17.9827	18.0457	20.2023	20.2342
50	5	14.1390	14.1421	29.3925	29.4256	32.4804	32.4796	25.8975	25.9285	27.6118	27.6443
	10	11.8652	11.8649	24.6645	24.6863	28.2604	28.2406	20.4143	20.4352	22.5374	22.5568
	20	11.2192	11.2179	23.3213	23.3398	27.0953	27.0696	18.7715	18.7894	21.0639	21.0786

Table 4 Validation of the first three natural frequencies (in Hz) of FG-GPLRC plate integrated with PZT-4 layers

B.Cs	Pattern	Electrical B.Cs	ω_1^*		ω_2^*		ω_3^*	
			[66]	Present	[66]	Present	[66]	Present
SSSS	FG-U	Closed	194.6542	193.4080	473.0629	471.6230	737.1725	737.1356
		Open	212.4215	208.8136	513.9120	506.6975	797.6343	788.5238
	FG-X	Closed	200.7564	199.4330	487.2087	485.7372	758.2765	758.3910
		Open	217.9551	214.3512	526.5769	519.5653	816.3174	807.7727
	FG-O	Closed	188.3221	187.1678	458.3229	456.9536	715.1009	714.9752
		Open	206.7111	203.1059	500.7897	493.3885	778.2083	768.5541
	FG-V	Closed	193.3006	192.1662	469.8815	468.6736	732.3669	732.6376
		Open	211.3362	207.7056	511.3930	504.0823	793.8719	784.5564
SCSC	FG-U	Closed	277.1016	276.5467	515.3822	515.0804	632.1755	634.7512
		Open	300.6491	294.6575	558.0915	550.4271	680.6446	671.5191
	FG-X	Closed	285.2832	284.7300	530.2858	530.0481	649.2736	652.1699
		Open	307.9534	302.1972	571.3338	564.0734	695.5870	687.3960
	FG-O	Closed	268.5684	268.0344	499.8134	499.4895	614.2148	616.5213
		Open	293.0748	286.8477	544.3397	536.2792	665.0458	654.9744
	FG-V	Closed	275.2803	274.8549	512.0238	511.9471	628.3063	631.0912
		Open	299.2117	293.1382	555.4525	547.6452	677.6558	668.2622
SFSF	FG-U	Closed	95.7410	95.0492	157.3421	156.5439	350.9796	349.8475
		Open	101.5868	100.0068	161.4380	159.9143	371.9132	367.7677
	FG-X	Closed	98.7446	98.0036	162.0779	161.2162	361.4859	360.2573
		Open	104.4177	102.8117	166.0412	164.4746	381.7233	377.5905
	FG-O	Closed	92.6313	91.9952	152.4396	151.7158	340.0707	339.0614
		Open	98.6659	97.1165	156.6804	155.2089	361.7656	357.6231
	FG-V	Closed	95.0854	94.4500	156.3207	155.6083	348.6398	347.6936
		Open	101.0143	99.4513	160.4764	159.0105	369.8982	365.7724

geometrical parameters are obtained and their accuracy are evaluated in comparison with those of reported by Van do and lee [65] which are tabulated in Table 3. Rectangular planform and 1 percent by weight fraction of GPL reinforcement are considered for development of results of this section.

Based on what can be seen from Table 3, it can be claimed that implementing the present theory and formulations for an FG-GPLRC cylindrical panel leads to excellent accuracy for results.

Next comparative study is carried out with the research performed by Majidi-Mozafari et al. [66] in which through an analytical approach, the free vibrations of sandwich plates reinforced with graphene nanoplatelets were investigated. To do so, the first three natural frequencies of FG-GPLRC plate with PZT-4 piezoelectric layer for various types of electrical and mechanical boundary conditions are computed and compared with those reported by Majidi–Mozafari et al. [66]. Table 4 shows the results of this comparison study. PZT-4 is considered as the piezoelectric material, and following data are considered to perform such comparison study: $W_{GPL} = 0.5\%$, $a/b = 1$, $a/h = 20$, $h/h^p = 20$.

As Table 4 also confirms, again for free vibration analysis of the structures surrounded by piezoelectric layers, the current model provides remarkable accuracy.

Now that through performing a number of comparison studies, the required confidence in the accuracy and correctness of the results has been attained; by providing novel numerical data, parametric studies are planned

Table 5 Variation of the first four frequency parameters in CCCC panels versus changing the number of layers with symmetric distribution of GPLs

Pattern	N_L	Electrical B.Cs	Ω_1	Ω_2	Ω_3	Ω_4
FG-U	2	Open	29.6031	56.5545	56.9060	80.6435
		Closed	28.0081	53.5947	53.9650	76.6631
	6	Open	29.6031	56.5545	56.9060	80.6435
		Closed	28.0081	53.5947	53.9650	76.6631
	10	Open	29.6031	56.5545	56.9060	80.6435
		Closed	28.0081	53.5947	53.9650	76.6631
	14	Open	29.6031	56.5545	56.9060	80.6435
		Closed	28.0081	53.5947	53.9650	76.6631
	16	Open	29.6031	56.5545	56.9060	80.6435
		Closed	28.0081	53.5947	53.9650	76.6631
	20	Open	29.6031	56.5545	56.9060	80.6435
		Closed	28.0081	53.5947	53.9650	76.6631
FG-X	2	Open	29.6031	56.5545	56.9060	80.6435
		Closed	28.0081	53.5947	53.9650	76.6631
	6	Open	30.3363	57.9163	58.2632	82.4847
		Closed	28.8002	55.0856	55.4498	78.6932
	10	Open	30.3938	58.0227	58.3693	82.6284
		Closed	28.8623	55.2019	55.5657	78.8513
	14	Open	30.4096	58.0520	58.3985	82.6679
		Closed	28.8793	55.2339	55.5975	78.8948
	16	Open	30.4135	58.0592	58.4056	82.6776
		Closed	28.8835	55.2417	55.6053	78.9054
	20	Open	30.4180	58.0676	58.4140	82.6889
		Closed	28.8884	55.2508	55.6145	78.9178
FG-O	2	Open	29.6031	56.5545	56.9060	80.6435
		Closed	28.0081	53.5947	53.9650	76.6631
	6	Open	28.8425	55.1329	55.4897	78.7153
		Closed	27.1834	52.0317	52.4088	74.5275
	10	Open	28.7804	55.0164	55.3736	78.5570
		Closed	27.1159	51.9032	52.2810	74.3517
	14	Open	28.7632	54.9842	55.3416	78.5132
		Closed	27.0972	51.8678	52.2457	74.3031
	16	Open	28.7590	54.9763	55.3337	78.5026
		Closed	27.0927	51.8591	52.2371	74.2913
	20	Open	28.7541	54.9671	55.3245	78.4900
		Closed	27.0873	51.8489	52.2269	74.2773

with the aim of evaluating the effects of the number of GPLRC layers, GPL weight fraction, structure curvature, mechanical boundary conditions and piezoelectric layer thickness on the characteristics of free vibrations of the FG-GPLRC cylindrical panel surrounded with piezoelectric layers. It should to be noted that hereafter a frequency parameter with definition of $\Omega = \omega a^2/h\sqrt{\rho_m/E_m}$ is used to present results.

The effects of the number of GPLRC layers on the first five frequency parameters of completely clamped FG-GPLRC cylindrical panel with symmetric (FG-U, FG-X, FG-O) and asymmetric (FG-V, FG-A) GPL distributions are illustrated in Tables 5 and 6. For better grasp, the first frequency parameters are also depicted in Fig. 3 for open circuit electrical boundary conditions. In this case study, the reinforcing parameter is fixed as $W_{GPL} = 0.5\%$.

It is evident that the first natural frequency of FG-U panel, which is a homogeneous model, is not affected by the number of layers; whereas by increasing the number of layers ascending trend is observed in variation of frequencies of FG-X model, descending trend can be seen for FG-O, FG-V and FG-A model. The same behavior is seen for higher frequencies.

This behavior, which is same to that observed for higher frequencies, is caused by the fact that the greater the distribution of GPLs in the outer layers, the greater the bending stiffness of the structure and subsequently the natural frequency of the structure. Besides, as Fig. 3 shows, frequencies hardly change when the number

Table 6 Variation of the first four frequency parameters Ω in CCCC panels versus changing the number of layers with asymmetric distribution of GPLs

Pattern	N_L	Electrical B.Cs	Ω_1	Ω_2	Ω_3	Ω_4
FG-V	2	Open	29.5061	56.3464	56.7215	80.3703
		Closed	27.8950	53.3542	53.7538	76.3499
	6	Open	29.4387	56.2118	56.5941	80.1892
		Closed	27.8188	53.2012	53.6097	76.1442
	10	Open	29.4326	56.1996	56.5825	80.1728
		Closed	27.8118	53.1873	53.5965	76.1254
	14	Open	29.4309	56.1962	56.5792	80.1682
		Closed	27.8099	53.1834	53.5929	76.1202
	16	Open	29.4304	56.1953	56.5784	80.1670
		Closed	27.8094	53.1825	53.5920	76.1189
	20	Open	29.4300	56.1944	56.5775	80.1657
		Closed	27.8088	53.1814	53.5909	76.1174
FG-A	2	Open	29.5004	56.3859	56.7150	80.4005
		Closed	27.9006	53.4134	53.7560	76.3945
	6	Open	29.4313	56.2627	56.5855	80.2282
		Closed	27.8259	53.2776	53.6124	76.2017
	10	Open	29.4250	56.2514	56.5737	80.2124
		Closed	27.8191	53.2651	53.5992	76.1840
	14	Open	29.4233	56.2482	56.5704	80.2079
		Closed	27.8171	53.2616	53.5956	76.1791
	16	Open	29.4228	56.2475	56.5696	80.2069
		Closed	27.8167	53.2608	53.5947	76.1779
	20	Open	29.4223	56.2466	56.5686	80.2056
		Closed	27.8161	53.2598	53.5936	76.1765

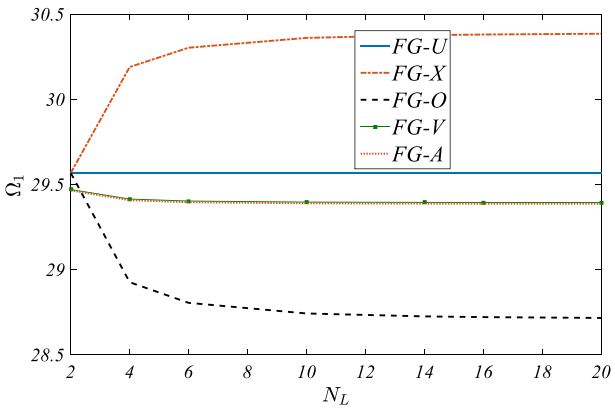

Fig. 3 Variations of fundamental frequency parameter Ω_1 by adding the number of layers

of layers is greater than 14. Thus, an FG-GPLRC panel with 10 layers may serve as a panel with continuous change of properties. Subsequently, the next results are obtained for a panel with 10 GPLRC layers.

The effects of the mechanical and electrical boundary conditions on the first five frequency parameters for FG-GPLRC cylindrical panel integrated with piezoelectric layers are investigated in Tables 7 and 8. 0.5 percent by weight of GPL reinforcement is considered. As demonstrated in these tables, panels with more edge constraints shows more natural frequencies. The observation that the frequencies are maximum for CCCC panel and are minimum for the CFFF panel supports this claim. As the second observation from Tables 7 and 8, the FG-GPLRC cylindrical panel with piezoelectric layers under open circuit condition has greater natural frequencies than the case with closed circuit condition. That is because during panel vibration, piezoelectric layers with open circuit boundary condition convert the electric potential into mechanical energy, while piezoelectric layers with closed circuit boundary conditions don't have this capability so evacuate the electrical energy.

Table 7 The effect of electrical and mechanical boundary conditions on first four frequency parameters of FG-GPLRC cylindrical panel with piezoelectric layers in symmetric distribution of GPLS

Pattern	Mechanical B.Cs	Electrical B.Cs	Ω_1	Ω_2	Ω_3	Ω_4
FG-U	SSSS	Closed	15.8703	37.8015	38.2317	59.1970
		Open	17.0722	40.5804	40.975	63.2547
	SFSF	Closed	7.5780	12.4558	28.5567	29.9998
		Open	8.0623	12.7715	29.9479	31.7083
	SCSF	Closed	10.0480	25.6504	31.9832	34.9438
		Open	10.4843	27.0081	33.6456	34.9438
	SCSC	Closed	22.4757	41.3223	51.2371	68.4726
		Open	23.8998	44.1236	54.1299	69.8855
	CCCC	Closed	28.0081	53.5947	53.965	76.6631
		Open	29.6031	56.5545	56.906	80.6435
	CFFF	Closed	2.7602	6.5646	16.4766	21.2698
		Open	3.1335	6.7409	17.1047	22.4548
	FCFF	Closed	2.8830	6.5883	16.7622	20.9953
		Open	3.2410	6.7642	17.3241	22.2535
	CCFF	Closed	5.5301	18.4561	20.5969	35.6800
		Open	5.8126	18.9054	21.8083	36.9392
FG-X	SSSS	Closed	16.3904	39.0533	39.4717	61.0824
		Open	17.5522	41.7236	42.1092	64.9660
	SFSF	Closed	7.8388	12.8676	29.4640	30.9972
		Open	8.3071	13.1723	30.8065	32.6407
	SCSF	Closed	10.3772	26.4626	33.0368	34.9461
		Open	10.7989	27.7699	34.6353	34.9461
	SCSC	Closed	23.191	42.6501	52.7769	69.8902
		Open	24.5608	45.3365	55.5371	69.8902
	CCCC	Closed	28.8623	55.2019	55.5657	78.8513
		Open	30.3938	58.0227	58.3693	82.6284
	CFFF	Closed	2.8565	6.7791	17.0223	21.9642
		Open	3.2185	6.9495	17.6271	22.8284
	FCFF	Closed	2.9748	6.8033	17.3016	21.6992
		Open	3.3228	6.9733	17.8454	22.9122
	CCFF	Closed	5.7084	19.0443	21.2680	36.7810
		Open	5.9821	19.4766	22.4362	37.9878
FG-O	SSSS	Closed	15.3307	36.4952	36.9386	57.2229
		Open	16.5766	39.3937	39.7983	61.4724
	SFSF	Closed	7.3074	12.0286	27.6141	28.9607
		Open	7.8094	12.3567	29.059	30.7409
	SCSF	Closed	9.7067	24.8048	30.8851	34.9461
		Open	10.1591	26.218	32.6181	34.9461
	SCSC	Closed	21.7292	39.9334	49.6185	66.3243
		Open	23.2132	42.8614	52.6575	69.8901
	CCCC	Closed	27.1159	51.9032	52.2810	74.3517
		Open	28.7804	55.0164	55.3736	78.5570
	CFFF	Closed	2.6604	6.3420	15.9090	20.5485
		Open	3.0462	6.5249	16.5632	21.7766
	FCFF	Closed	2.7880	6.3653	16.2021	20.2634
		Open	3.1570	6.5478	16.7837	21.5714
	CCFF	Closed	5.3454	17.8446	19.8979	34.5303
		Open	5.6376	18.3127	21.1567	35.8475

Tables 9 and 10 show the variation of first four frequency parameters of the SCSC FG-GPLRC panel versus the weight fraction of augmented GPLs to epoxy matrix for different GPL distribution pattern. Needless to more discuss, adding more GPL to the epoxy matrix leads to more increase in natural frequencies. The feature has been verified in many of the studies on GPLRC structures; see, e.g., [67–73]. This is due to the fact the elasticity modulus of GPL is much higher than that of Epoxy. The increasing rate is higher for the FG-X pattern and lower for the FG-O pattern as depicted in Fig. 4. The reason for this observation can be found in the greater bending stiffness of FG-X model and the less bending stiffness of the FG-O model.

The effect of piezoelectric layer thickness-to-panel thickness ratio on the natural frequency of the SCSC FG-GPLRC cylindrical panel surrounded with piezoelectric layers with open/closed electrical boundary condition

Table 8 The effect of electrical and mechanical boundary conditions on first four frequency parameters of FG-GPLRC cylindrical panel with piezoelectric layers in asymmetric distribution of GPLS

Pattern	Mechanical B.Cs	Electrical B.Cs	Ω_1	Ω_2	Ω_3	Ω_4
FG-V	SSSS	Closed	15.7553	37.4899	37.9543	58.7403
		Open	16.9828	40.3182	40.7369	62.8605
	SFSF	Closed	7.5124	12.3630	28.3597	29.7452
		Open	8.0189	12.6931	29.7697	31.4910
	SCSF	Closed	9.9693	25.4734	31.7167	34.9637
		Open	10.4227	26.8525	33.4151	34.9637
	SCSC	Closed	22.3121	40.9917	50.8837	67.9748
		Open	23.7622	43.8427	53.8205	69.9235
	CCCC	Closed	27.8118	53.1873	53.5965	76.1254
		Open	29.4326	56.1996	56.5825	80.1728
	CFFF	Closed	2.7382	6.5141	16.3314	21.1118
		Open	3.1108	6.6939	16.9763	22.3164
	FCFF	Closed	2.8630	6.5410	16.6433	20.8195
		Open	3.2196	6.7205	17.2170	22.1023
	CCFF	Closed	5.4898	18.3125	20.4366	35.4220
		Open	5.7741	18.7739	21.6707	36.7025
FG-A	SSSS	Closed	15.7519	37.5430	37.9442	58.7841
		Open	16.9523	40.3358	40.7103	62.8796
	SFSF	Closed	7.5283	12.3686	28.3443	29.8052
		Open	7.9998	12.6767	29.7456	31.5153
	SCSF	Closed	9.9819	25.4618	31.7753	34.9280
		Open	10.4099	26.8276	33.4401	34.9280
	SCSC	Closed	22.3169	41.0471	50.8849	68.0248
		Open	23.7470	43.8652	53.8093	69.8522
	CCCC	Closed	27.8191	53.2651	53.5992	76.1840
		Open	29.4250	56.2514	56.5737	80.2124
	CFFF	Closed	2.7395	6.5219	16.3785	21.1142
		Open	3.1194	6.6978	17.0041	22.3037
	FCFF	Closed	2.8623	6.5422	16.6411	20.8530
		Open	3.2269	6.7176	17.2025	22.1136
	CCFF	Closed	5.4923	18.3390	20.4546	35.4419
		Open	5.7778	18.7862	21.6695	36.7100

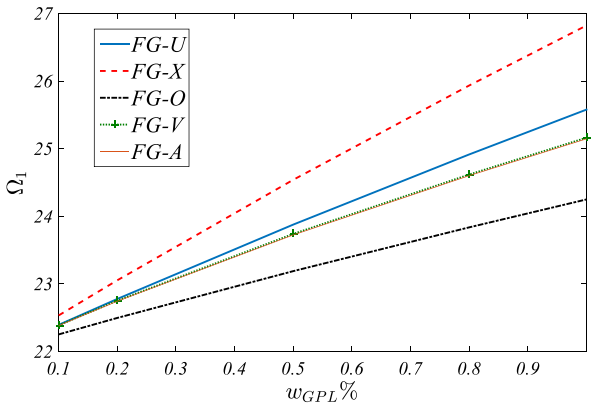

Fig. 4 Variation of the first frequency parameter with respect to adding more GPL to epoxy matrix in SCSC panels

Table 9 The effect of GPL weigh fractions on first four frequency parameters of SCSC FG-GPLRC cylindrical panel surrounded with PZT layers with symmetric pattern

Pattern	$W_{GPL}\%$	Electrical B.Cs	Ω_1	Ω_2	Ω_3	Ω_4
FG-U	0.1	Closed	20.9304	38.5150	47.5722	60.6383
		Open	22.4190	41.4257	50.5461	60.6383
	0.2	Closed	21.3296	39.2409	48.5238	63.0758
		Open	22.8019	42.1248	51.4797	63.0758
	0.5	Closed	22.4757	41.3223	51.2371	68.4726
		Open	23.8998	44.1236	54.1299	69.8855
	0.8	Closed	23.5574	43.2844	53.7788	71.8773
		Open	24.9358	46.0041	56.6024	75.7725
	1.0	Closed	24.2487	44.5374	55.3958	74.0419
		Open	25.5981	47.2047	58.1728	77.8767
FG-X	0.1	Closed	21.0836	38.7982	47.8981	60.6385
		Open	22.5585	41.6802	50.8390	60.6385
	0.2	Closed	21.6305	39.7980	49.1664	63.0766
		Open	23.0771	42.6277	52.0600	63.0766
	0.5	Closed	23.1910	42.6501	52.7769	69.8902
		Open	24.5608	45.3365	55.5371	69.8902
	0.8	Closed	24.6500	45.3167	56.1444	75.0162
		Open	25.9534	47.8776	58.7848	76.1070
	1.0	Closed	25.5755	47.0081	58.2774	77.8681
		Open	26.8393	49.4939	60.8451	79.9894
FG-O	0.1	Closed	20.7758	38.2289	47.2423	60.6385
		Open	22.2782	41.1688	50.2502	60.6385
	0.2	Closed	21.0229	38.6726	47.8666	63.0766
		Open	22.5219	41.6129	50.8877	63.0766
	0.5	Closed	21.7292	39.9334	49.6185	66.3243
		Open	23.2132	42.8614	52.6575	69.8901
	0.8	Closed	22.3953	41.1148	51.2365	68.4964
		Open	23.8598	44.0180	54.2717	72.6953
	1.0	Closed	22.8220	41.8690	52.2600	69.8668
		Open	24.2723	44.7516	55.2852	74.0584

Table 10 The effect of GPL weigh fractions on first four frequency parameters of SCSC FG-GPLRC cylindrical panel surrounded with PZT layers with asymmetric pattern

Pattern	$W_{GPL}\%$	Electrical B.Cs	Ω_1	Ω_2	Ω_3	Ω_4
FG-V	0.1	Closed	20.9211	38.4912	47.5530	60.6466
		Open	22.4135	41.4087	50.5311	60.6466
	0.2	Closed	21.2959	39.1660	48.4526	63.0918
		Open	22.7769	42.0660	51.4203	63.0918
	0.5	Closed	22.3121	40.9917	50.8837	67.9748
		Open	23.7622	43.8427	53.8205	69.9235
	0.8	Closed	23.2182	42.6150	53.0384	70.8518
		Open	24.6395	45.4188	55.9418	74.8631
	1.0	Closed	23.7804	43.6203	54.3687	72.6268
		Open	25.1832	46.3931	57.2482	76.6104
FG-A	0.1	Closed	20.9215	38.5047	47.5519	60.6302
		Open	22.4083	41.4129	50.5267	60.6302
	0.2	Closed	21.2971	39.1916	48.4513	63.0603
		Open	22.7680	42.0747	51.4129	63.0603
	0.5	Closed	22.3169	41.0471	50.8849	68.0248
		Open	23.7470	43.8652	53.8093	69.8522
	0.8	Closed	23.2276	42.6937	53.0445	70.925
		Open	24.6227	45.4548	55.9313	74.9082
	1.0	Closed	23.7931	43.7123	54.3787	72.7138
		Open	25.1668	46.4378	57.2397	76.6663

Table 11 Variations of the first four frequency parameters of FG-GPLRC cylindrical panel versus the ratio of h^p/h

Pattern	h^p/h	Electrical B.Cs	Ω_1	Ω_2	Ω_3	Ω_4
FG-U	0.01	Closed	17.0431	31.2411	39.1466	52.397
		Open	17.5897	32.3375	40.3127	54.0243
	0.02	Closed	18.8627	34.6348	43.2340	57.8493
		Open	19.7427	36.3882	45.0814	60.4163
	0.05	Closed	22.4757	41.3223	51.2371	68.4726
		Open	23.8998	44.1236	54.1299	69.8855
	0.1	Closed	23.7470	43.8652	53.8093	69.8522
		Open	26.0687	47.9120	59.0300	72.8751
FG-X	0.01	Closed	18.4339	33.8586	42.2413	56.5325
		Open	18.9316	34.8505	43.2869	57.9860
	0.02	Closed	19.9889	36.7435	45.7114	61.1494
		Open	20.8096	38.3706	47.4129	63.5069
	0.05	Closed	23.1910	42.6501	52.7769	69.8902
		Open	24.5608	45.3365	55.5371	69.8902
	0.1	Closed	26.5029	48.7118	59.9442	72.8783
		Open	28.2975	52.1817	63.4312	72.8783
FG-U	0.01	Closed	15.4976	28.3116	35.6523	47.7072
		Open	16.1072	29.5444	36.9750	49.5612
	0.02	Closed	17.6452	32.3440	40.5226	54.2262
		Open	18.5964	34.2499	42.5457	57.0466
	0.05	Closed	21.7292	39.9334	49.6185	66.3243
		Open	23.2132	42.8614	52.6575	69.8901
	0.1	Closed	25.6244	47.0927	58.0907	72.8783
		Open	27.4993	50.7320	61.7717	72.8783
FG-V	0.01	Closed	16.5002	30.1870	37.9252	50.7253
		Open	17.0784	31.3469	39.1556	52.4457
	0.02	Closed	18.4907	33.9067	42.4085	56.7128
		Open	19.4051	35.7281	44.3222	59.3762
	0.05	Closed	22.3121	40.9917	50.8837	67.9748
		Open	23.7622	43.8427	53.8205	69.9235
	0.1	Closed	26.0021	47.7691	58.8909	72.9020
		Open	27.8516	51.3508	62.4952	72.9020
FG-A	0.01	Closed	16.5171	30.2603	37.9449	50.8007
		Open	17.0810	31.3975	39.1658	52.5059
	0.02	Closed	18.5017	33.9747	42.4189	56.7790
		Open	19.3973	35.7657	44.3204	59.4222
	0.05	Closed	22.3169	41.0471	50.8849	68.0248
		Open	23.7470	43.8652	53.8093	69.8522
	0.1	Closed	26.0050	47.8116	58.8902	72.8526
		Open	27.8386	51.3669	62.4848	72.8526

is studied in Table 11 and for first frequency parameter of X-GPLRC panel is displayed in Fig. 5. It can be seen that panels with thicker piezoelectric layers experience higher natural frequencies. Also, Fig. 5 reveals that natural frequencies of the panels with open circuit electrical boundary conditions are more sensitive to the thickness of piezoelectric layer than those with closed circuit electrical boundary conditions.

Table 12 represents variation of frequency parameters versus R/a ratio of the SCSC FG-GPLRC panel with $W_{GPL} = 0.5\%$ for different GPL distribution patterns. It is observed that increasing panel curvature leads to growing the frequencies as a consequence of increasing configuration stiffness.

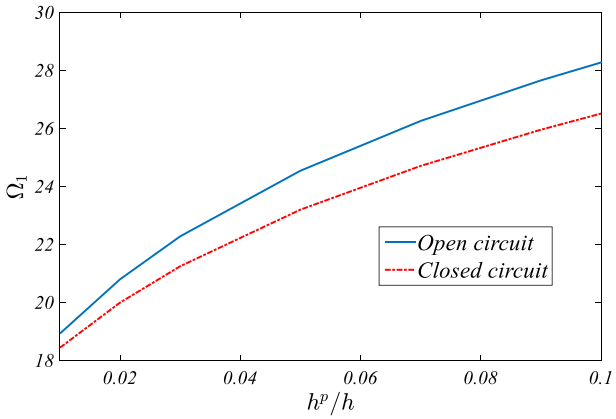

Fig. 5 How the first frequency parameter is affected by piezoelectric layer thickness changes

Table 12 The effect of R/a on first four frequency parameters of the FG-GPLRC panel with top and bottom piezoelectric layers

Pattern	R/a	Electrical B.Cs	Ω_1	Ω_2	Ω_3	Ω_4
FG-U	3	Closed	22.9833	41.3235	51.7584	68.5677
		Open	24.3969	44.1383	54.6217	69.8857
	5	Closed	22.4757	41.3223	51.2371	68.4726
		Open	23.8998	44.1236	54.1299	69.8855
	10	Closed	22.2566	41.3219	51.0151	68.4323
		Open	23.6857	44.1174	53.9206	69.8855
	20	Closed	22.2014	41.3217	50.9595	68.4223
		Open	23.6317	44.1159	53.8681	69.8854
FG-X	3	Closed	23.6782	42.6456	53.2798	69.8904
		Open	25.0402	45.3458	56.0135	69.8904
	5	Closed	23.1910	42.6501	52.7769	69.8902
		Open	24.5608	45.3365	55.5371	69.8902
	10	Closed	22.9811	42.6521	52.5629	69.8901
		Open	24.3545	45.3326	55.3345	69.8901
	20	Closed	22.9281	42.6526	52.5092	69.8901
		Open	24.3025	45.3316	55.2836	69.8901
FG-O	3	Closed	22.2595	39.9407	50.1603	66.4286
		Open	23.7296	42.8819	53.1662	69.8902
	5	Closed	21.7292	39.9334	49.6185	66.3243
		Open	23.2132	42.8614	52.6575	69.8901
	10	Closed	21.5001	39.9303	49.3877	66.2802
		Open	22.9904	42.8527	52.4409	69.8901
	20	Closed	21.4423	39.9295	49.3298	66.2691
		Open	22.9343	42.8505	52.3866	69.8901
FG-V	3	Closed	22.8225	40.9760	51.4086	68.0554
		Open	24.2674	43.8513	54.3192	69.9474
	5	Closed	22.3121	40.9917	50.8837	67.9748
		Open	23.7622	43.8427	53.8205	69.9235
	10	Closed	22.0922	41.0044	50.6603	67.9462
		Open	23.5426	43.8416	53.6070	69.9056
	20	Closed	22.0370	41.0111	50.6042	67.9422
		Open	23.4862	43.8427	53.5527	69.8967
FG-A	3	Closed	22.8314	41.0679	51.4111	68.1385
		Open	24.2439	43.8886	54.3012	69.8286
	5	Closed	22.3169	41.0471	50.8849	68.0248
		Open	23.7470	43.8652	53.8093	69.8522
	10	Closed	22.0945	41.0322	50.6608	67.9712
		Open	23.5348	43.8529	53.6013	69.8700
	20	Closed	22.0381	41.0250	50.6045	67.9547
		Open	23.4823	43.8484	53.5499	69.8789

7 Conclusions

The present work deals with free vibrations of functionally graded graphene platelet-reinforced cylindrical panels completely surrounded with top and bottom piezoelectric layers. Mechanical properties of GPLRC layers were estimated in accordance with modified Halpin–Tsai micromechanical model, rule of mixtures and the concept of layer-wise functionally graded distribution of GPLs. Hamilton principle was utilized to obtain coupled PDEs of motions on the basis of FSDT and Maxwell equation. With the aid of Legendre-Ritz technique, spatial domain was discretized and inertia and equivalent stiffness matrix were calculated. Through a number of comparison studies, the accuracy of present solution procedure was validated and subsequently novel numerical data were generated to establish the parameter studies. Some conclusions are outlined as:

- Increasing the number of layers leads to an increase in frequency for the FG-X pattern and a decrease in frequency for FG-O and asymmetric patterns. However, the change in frequencies is negligible when the number of layers is greater than 10. As a result, a panel with only 10 layers may serve as a panel with continuous change of GPL weight fraction.
- As the piezoelectric layer becomes thicker frequencies show more dependency on electric boundary conditions, for thinner piezoelectric layer, frequency parameters grow rapidly with thickening piezoelectric layer.
- Deeper panel has higher natural frequencies.
- In general, increasing the GPL weight fraction or exploiting models with more dispersion of GPLs in the outer layers leads to an enrichment of the panel stiffness and, as a result, a growth in natural frequencies.
- FG-X panel has the maximum frequencies, and FG-O panel has the minimum frequencies
- Open circuit condition results in higher frequencies.

References

1. Golabchi, H., Kolahchi, R., Rabani Bidgoli, M.: Vibration and instability analysis of pipes reinforced by SiO_2 nanoparticles considering agglomeration effects. Comput. Concr. **21**(4), 431–440 (2018)
2. Kargarzadeh, H., Mariano, M., Huang, J., Lin, N., Ahmad, I., Dufresne, A., Thomas, S.: Recent developments on nanocellulose reinforced polymer nanocomposites: a review. Polymer **132**, 368–393 (2017)
3. Garcia, C., Trendafilova, I., Zucchelli, A.: The effect of polycaprolactone nanofibers on the dynamic and impact behavior of glass fibre reinforced polymer composites. J. Compos. Sci. **2**(3), 43 (2018)
4. Mirzaei, M., Kiani, Y.: Free vibration of functionally graded carbon-nanotube-reinforced composite plates with cutout. Beilstein J. Nanotechnol. **7**, 511–523 (2016)
5. Mirzaei, M., Kiani, Y.: Free vibration of functionally graded carbon nanotube reinforced composite cylindrical panels. Compos. Struct. **142**, 45–56 (2016)
6. Kiani, Y.: Free vibration of FG-CNT reinforced composite skew plates. Aerosp. Sci. Technol. **58**, 178–188 (2016)
7. Zhang, L.W., Liew, K.M.: Large deflection analysis of FG-CNT reinforced composite skew plates resting on Pasternak foundations using an element-free approach. Compos. Struct. **132**, 974–983 (2015)
8. Kumar, R., Kumar, A.: Free vibration response of cnt-reinforced multiscale functionally graded plates using the modified shear deformation theory. Adv. Mater. Process. Technol. **8**(4), 4257–4279 (2022)
9. Biswas, S., Datta, P.: Finite element model for free vibration analyses of FG-CNT reinforced composite beams using refined shear deformation theories. IOP Conf. Ser. Mater. Sci. Eng. 1206, Article Number 012019 (2019)
10. Truong-Thi, T., Vo-Duy, T., Ho-Huu, V., Nguyen-Thoi, T.: Static and free vibration analyses of functionally graded carbon nanotube reinforced composite plates using CS-DSG3. Int. J. Comput. Methods **17**(3), 1850133 (2020)
11. Mirjavadi, S.S., Forsat, M., Barati, M.R., Hamouda, A.M.S.: Analysis of nonlinear vibrations of CNT-/fiberglass-reinforced multi-scale truncated conical shell segments. Mech. Based Des. Struct. Mach. **50**(6), 2067–2083 (2022)
12. Novoselov, K.S., Geim, A.K., Morozov, S.V., Jiang, D., Zhang, Y., Dubonos, S.V., Grigorieva, I.V., Firsov, A.A.: Electric filed effect in atomically thin carbon films. Science **306**, 666–669 (2004)
13. Rafiee, M.A., Rafiee, J., Yu, Z.Z., Koratkar, N.: Buckling resistant graphene nanocomposites. Appl. Phys. Lett. **95**, 223103 (2009)
14. Biswas, S., Fukushima, H., Drzal, L.T.: Mechanical and electrical property enhancement in exfoliated graphene nanoplatelet/liquid crystalline polymer nanocomposites. Compos. A Appl. Sci. Manuf. **42**, 371–375 (2011)
15. Parashar, A., Mertiny, P.: Representative volume element to estimate buckling behavior of graphene/polymer nanocomposite. Nanoscale Res. Lett. **7**, 515 (2012)
16. Zhao, S., Zhao, Z., Yang, Z., Ke, L.L., Kitipornchai, S., Yang, J.: Functionally graded graphene reinforced composite structures: a review. Eng. Struct. **210**, 110339 (2020)
17. Zhao, Z., Feng, C., Wang, Y., Yang, J.: Bending and vibration analysis of functionally graded trapezoidal nanocomposite plates reinforced with graphene nanoplatelets (GPLs). Compos. Struct. **180**, 799–808 (2017)
18. Song, M.T., Yang, J., Kitipornchai, S., Zhu, W.D.: Buckling and postbuckling of biaxially compressed functionally graded multilayer graphene nanoplatelet-reinforced polymer composite plates. Int. J. Mech. Sci. **131–132**, 345–355 (2017)
19. Wang, Y., Feng, C., Zhao, Z., Yang, J.: Eigenvalue buckling of functionally graded cylindrical shells reinforced with graphene platelets (GPL). Compos. Struct. **202**, 38–46 (2018)

20. Wu, H.L., Yang, J., Kitipornchai, S.: Dynamic instability of functionally graded multilayer graphene nanocomposite beams in thermal environment. Compos. Struct. **162**, 244–254 (2017)
21. Wang, Y., Feng, C., Wang, X.W., Zhao, Z., Romero, C.S., Dong, Y.H., Yang, J.: Nonlinear static and dynamic responses of graphene platelets reinforced composite beam with dielectric permittivity. Appl. Math. Model. **71**, 298–315 (2019)
22. Ganapathi, M., Aditya, S., Shubhendu, S., Polit, O., Ben, Z.T.: Nonlinear supersonic flutter study of porous 2D curved panels including graphene platelets reinforcement effect using trigonometric shear deformable finite element. Int. J. Non-Linear Mech. **125**, 103543 (2020)
23. Shen, H.S., Xiang, Y., Lin, F.: Nonlinear bending of functionally graded graphene-reinforced composite laminated plates resting on elastic foundations in thermal environments. Compos. Struct. **170**, 80–90 (2017)
24. Shen, H.S., Xiang, Y.: Thermal buckling and postbuckling behavior of FG-GRC laminated cylindrical shells with temperature-dependent material properties. Meccanica **54**, 283–297 (2019)
25. Shen, H.S., Xiang, Y., Lin, F.: A novel technique for nonlinear dynamic instability analysis of FG-GRC laminated plates. Thin-Walled Struct. **139**, 389–397 (2019)
26. Lin, F., Xiang, Y., Shen, H.S.: Nonlinear forced vibration of FG-GRC laminated plates resting on visco-Pasternak foundations. Compos. Struct. **209**, 443–452 (2019)
27. Gholami, R., Ansari, R.: Nonlinear harmonically excited vibration of third-order shear deformable functionally graded graphene platelet-reinforced composite rectangular plates. Eng. Struct. **156**, 197–209 (2018)
28. Gholami, R., Ansari, R.: On the nonlinear vibrations of polymer nanocomposite rectangular plates reinforced by graphene nanoplatelets: a unified higher-order shear deformable model. Iran. J. Sci. Technol. Trans. Mech. Eng. **43**, 603–620 (2019)
29. Zhou, Z., Ni, Y., Tong, Z., Zhu, S., Sun, J., Xu, X.: Accurate nonlinear buckling analysis of functionally graded porousgraphene platelet reinforced composite cylindrical shells. Int. J. Mech. Sci. **151**, 537–550 (2019)
30. Song, M., Kitipornchai, S., Yang, J.: Free and forced vibrations of functionally graded polymer composite plates reinforced with graphene nanoplatelets. Compos. Struct. **159**, 579–588 (2017)
31. Baghbadorani, A.A.M., Kiani, Y.: Vibration analysis of functionally graded cylindrical shells reinforced with graphene platelets. Compos. Struct. **276**, 114546 (2021)
32. Esmaeili, H.R., Kiani, Y., Tadi Beni, Y.: Vibration characteristics of composite doubly curved shells reinforced with graphene platelets with arbitrary edge supports. Acta Mech. **233**(2), 1–19 (2022)
33. Esmaeili, H.R., Kiani, Y.: On the response of graphene platelet reinforced composite laminated plates subjected to instantaneous thermal shock. Eng. Anal. Bound. Elem. **141**, 167–180 (2022)
34. Esmaeili, H.R., Kiani, Y.: Vibrations of graphene platelet reinforced composite doubly curved shells subjected to thermal shock. Mech. Based Des. Struct. Mach. (2022). https://doi.org/10.1080/15397734.2022.2120499
35. Nguyen, N.V., Lee, J.: On the static and dynamic responses of smart piezoelectric functionally graded graphene platelet-reinforced microplates. Int. J. Mech. Sci. **197**, 106310 (2021)
36. Jalali, M.R., Shavalipour, A., Safarpour, M., Moayedi, H., Safarpour, H.: Frequency analysis of a graphene platelet–reinforced imperfect cylindrical panel covered with piezoelectric sensor and actuator. J. Strain Anal. Eng. Des. **55**(5–6), 181–196 (2020)
37. Dong, Y., Li, Y., Li, X., Yang, J.: Active control of dynamic behaviors of graded graphene reinforced cylindrical shells with piezoelectric actuator/sensor layers. Appl. Math. Model. **82**, 252–270 (2020)
38. Lin, H.G., Cao, D.Q., Xu, Y.Q.: Vibration, buckling and aeroelastic analyses of functionally graded multilayer graphene-nanoplatelets-reinforced composite plates embedded in piezoelectric layers. Int. J. Appl. Mech. **10**(3), 1850023 (2018)
39. Alibeigloo, A., Nouri, V.: Static analysis of functionally graded cylindrical shell with piezoelectric layers using differential quadrature method. Compos. Struct. **92**(8), 1775–1785 (2010)
40. Bayat, A., Jalali, A., Ahmadi, H.: Nonlinear dynamic analysis and control of FG cylindrical shell fitted with piezoelectric layers. Int. J. Struct. Stab. Dyn. **21**(06), 2150083 (2021)
41. Yang, J., Sun, G., Fu, G.: Bifurcation and chaos of functionally graded carbon nanotube reinforced composite cylindrical shell with piezoelectric layer. Mech. Solids **56**, 856–872 (2021)
42. Ebrahimi, Z.: Vibration and stability analysis of a functionally graded cylindrical shell embedded in piezoelectric layers conveying fluid flow. J. Vib. Control (2022). https://doi.org/10.1177/10775463221081184
43. Rabab, A., Alghanmi, A., Zenkour, M.: An electromechanical model for functionally graded porous plates attached to piezoelectric layer based on hyperbolic shear and normal deformation theory. Compos. Struct. **274**, 114352 (2021)
44. Markad, K.M., Das, V., Lal, A.: Deflection and stress analysis of piezoelectric laminated composite plate under variable polynomial transverse loading. AIP Adv. **12**, 085024 (2022)
45. Lore, S., Deshpande, S., Nath Singh, B.: Nonlinear free vibration analysis of functionally graded plates and shell panels using quasi-3D higher order shear deformation theory. Mech. Adv. Mater. Struct. (2022). https://doi.org/10.1080/15376494.2022.2114050
46. Li, X., Yu, K., Han, J., Zhao, R., Wu, Y.: A piecewise shear deformation theory for free vibration of composite and sandwich panels. Compos. Struct. **124**, 111–119 (2015)
47. Shen, H.S., Wang, H.: Nonlinear vibration of shear deformable FGM cylindrical panels resting on elastic foundations in thermal environments. Compos. B Eng. **60**, 167–177 (2014)
48. Viola, E., Tornabene, F., Fantuzzi, N.: General higher-order shear deformation theories for the free vibration analysis of completely doubly-curved laminated shells and panels. Compos. Struct. **95**, 639–666 (2013)
49. Chen, Y., Ye, T., Jin, G., Lee, H.P., Ma, X.: A unified quasi-three-dimensional solution for vibration analysis of rotating pre-twisted laminated composite shell panels. Compos. Struct. **282**, 115072 (2022)
50. Karami, B., Janghorban, M., Fahham, H.R.: Forced vibration analysis of anisotropic curved panels via a quasi-3D model in orthogonal curvilinear coordinate. Thin-Walled Struct. **175**, 109254 (2022)
51. Karimiasl, M., Alibeigloo, A.: Nonlinear aeroelastic analysis of sandwich composite cylindrical panel with auxetic core subjected to the thermal environment. J. Vib. Control. **1**, 2 (2022). https://doi.org/10.1177/10775463221094715
52. Pourmoayed, A.R., Malekzadeh Fard, K., Shahravi, M.: Vibration analysis of a cylindrical sandwich panel with flexible core using an improved higher-order theory. Latin Am. J. Solids Struct. **14**(4), 714–742 (2017)

53. Mohammadimehr, M., Okhravi, S., Akhavan Alavi, S.: Free vibration analysis of magneto-electro-elastic cylindrical composite panel reinforced by various distributions of CNTs with considering open and closed circuits boundary conditions based on FSDT. J. Vib. Control **24**(8), 1551–1569 (2016)
54. Keleshteri, M.M., Jelovica, J.: Analytical solution for vibration and buckling of cylindrical sandwich panels with improved FG metal foam core. Eng. Struct. **266**, 114580 (2022)
55. Nazemizadeh, M., Bakhtiarinejad, F., Assadi, A., Shahriari, B.: Nonlinear vibration of piezoelectric laminated nanobeams at higher modes based on nonlocal piezoelectric theory. Acta Mech. **231**, 4259–4274 (2020)
56. Civalek, O., Uzun, B., Yayli, M.O.: An effective analytical method for buckling solutions of a restrained FGM nonlocal beam. Comput. Appl. Math. **41**, 67 (2022)
57. Abouelregal, A.E., Ersoy, H., Civalek, O.: Solution of Moore–Gibson–Thompson equation of an unbounded medium with a cylindrical hole. Mathematics **9**(13), 1536 (2021)
58. Akgöz, B., Civalek, O.: Buckling analysis of functionally graded tapered microbeams via Rayleigh–Ritz method. Mathematics **10**(23), 4429 (2022)
59. Jalaei, M.H., Thai, H.T., Civalek, O.: On viscoelastic transient response of magnetically imperfect functionally graded nanobeams. Int. J. Eng. Sci. **172**, 103629 (2022)
60. Numanoglu, H.M., Ersoy, H., Akgöz, B., Civalek, O.: A new eigenvalue problem solver for thermo-mechanical vibration of Timoshenko nanobeams by an innovative nonlocal finite element method. Math. Methods Appl. Sci. **45**, 2592–2614 (2022)
61. Civalek, O., Dastjerdi, S., Akgoz, B.: Buckling and free vibrations of CNT-reinforced cross-ply laminated composite plates. Mech. Based Des. Struct. Mach. **50**(6), 1914–1931 (2022)
62. Sobhani, E., Arbabian, A., Civalek, O., Avkar, M.: The free vibration analysis of hybrid porous nanocomposite joined hemispherical-cylindrical-conical shells. Eng. Comput. **38**(4), 3125–3152 (2022)
63. Fan, T.: An energy harvester with nanoporous piezoelectric double-beam structure. Acta Mech. **233**, 1083–1098 (2022)
64. Olson, M.D., Lindberg, G.M.: Dynamic analysis of shallow shell with a doubly-curved triangular finite element. J. Sound Vib. **19**, 299–318 (1971)
65. Van Do, V., Lee, C.H.: Static bending and free vibration analysis of multilayered composite cylindrical and spherical panels reinforced with graphene platelets by using isogeometric analysis method. Eng. Struct. **215**, 110682 (2020)
66. Majidi-Mozafari, K., Bahaadini, R., Saidi, A.R., Khodabakhsh, R.: An analytical solution for vibration analysis of sandwich plates reinforced with graphene nanoplatelets. Eng. Comput. **38**, 2107–2123 (2020)
67. Guo, H., Zur, K.K., Ouyang, X.: New insights into the nonlinear stability of nanocomposite cylindrical panels under aero-thermal loads. Compos. Struct. **303**, 116231 (2023)
68. Guo, H., Ouyang, X., Zur, K.K., Wu, X., Yang, T., Ferreira, A.J.M.: On the large amplitude vibration of rotating pre-twisted graphene nanocomposite blades in a thermal environment. Compos. Struct. **282**, 115129 (2022)
69. Guo, H., Ouyang, X., Yang, T., Zur, K.K., Reddy, J.N.: On the dynamics of rotating cracked functionally graded blades reinforced with graphene nanoplatelets. Eng. Struct. **249**, 113286 (2021)
70. Guo, H., Ouyang, X., Zur, K.K., Wu, X.: Meshless numerical approach to flutter analysis of rotating pre-twisted nanocomposite blades subjected to supersonic airflow. Eng. Anal. Bound. Elem. **132**, 1–11 (2021)
71. Guo, H., Du, X., Zur, K.K.: On the dynamics of rotating matrix cracked FG-GPLRC cylindrical shells via the element free IMLS-Ritz method. Eng. Anal. Bound. Elem. **131**, 228–239 (2021)
72. Eyvazian, A., Sebaey, T.A., Zur, K.K., Khan, A., Zhang, H., Wong, S.H.F.: On the dynamics of FG-GPLRC sandwich cylinders based on an unconstrained higher-order theory. Compos. Struct. **267**, 113879 (2021)
73. Guo, H., Yang, T., Zur, K.K., Reddy, J., Ferreira, A.J.M.: Effect of thermal environment on nonlinear flutter of laminated composite plates reinforced with graphene nanoplatelets. Model. Comput. Vib. Probl. **1**, 1–32 (2021)